RESEARCH ARTICLE | JUNE 18 2026

Laser controlled combustion rate of an aluminum/copper oxide thermite

Touhid Bin Anwar ; Erik Hagen ; Keren Shi ; Michael R. Zachariah ; Christopher J. Bardeen

J. Appl. Phys. 139, 233104 (2026)
https://doi.org/10.1063/5.0330683

Journal of Applied Physics ARTICLE pubs.aip.org/aip/jap

Laser controlled combustion rate of an aluminum/copper oxide thermite

Cite as: J. Appl. Phys. **139**, 233104 (2026); doi: 10.1063/5.0330683
Submitted: 22 February 2026 · Accepted: 27 May 2026 ·
Published Online: 18 June 2026

View Online Export Citation CrossMark

Touhid Bin Anwar, Erik Hagen, Keren Shi, Michael R. Zachariah,[a] and Christopher J. Bardeen[a]

AFFILIATIONS

Department of Chemical Engineering, University of California, Riverside, California 92521, USA

[a]**Authors to whom correspondence should be addressed:** christob@ucr.edu and mrz@engr.ucr.edu

ABSTRACT

This study demonstrates that the burn rate of an Al/CuO nanothermite can be controlled using continuous wave laser irradiation. Expanding a 532 nm laser beam through a cylindrical lens enabled the creation of a spatially varying temperature increase of up to 200 °C across the surface of a 3D printed thermite stick. Temperature distributions on the surface were monitored using an infrared camera, and the velocity of the burning front was tracked with a high-speed camera. Two-color pyrometry showed that the flame temperature was not affected by laser illumination, so the burn rate increase is attributed to the increase in initial surface temperature of the thermite. The local velocity of the front could be increased by a factor of 3 by this photothermal heating. Effective activation energies were extracted from Arrhenius plots of local velocities vs surface temperatures. The measured activation energy of ~10 kJ/mol at the highest peak temperature probably reflects more facile mass transport in the heated regions. This study represents a proof-of-concept for measuring the temperature sensitivity of the local burn rates in nanothermite systems. It also demonstrates that visible laser irradiation provides a non-contact method to modulate combustion rates in solid-state energetic materials.

I. INTRODUCTION

Solid-state energetic materials are key ingredients in several important technologies,[1,2] including explosives and propellants. For rocket applications, solid propellants combine high energy densities with convenient and simple operation. Unlike liquid propellants, they do not require complex containment vessels and mixing mechanisms. After ignition, the exothermic reaction between premixed oxidizer and fuel produces sufficient internal heat to support the reaction until the fuel is completely consumed. This simplicity comes with a cost, however, since there is no convenient mechanism for modulating the reaction rate after ignition. This is a disadvantage because it is often desirable to actively control the thrust output of a rocket as it travels. For liquid fuel propellants, it is straightforward to control the reaction rate by using valves to regulate the ratio of oxidizer to fuel. If a general way to control the burn rate of solid propellants can be developed, this would remove one barrier to their wider use in rocket propulsion.

The problem of reaction rate control for solid-state energetic materials has motivated research into a variety of different strategies. One way to change the burn rate is to engineer different solid geometries into the propellant body,[3,4] but this passive strategy does not enable active control by an external source. Another strategy involves incorporating electrically powered heaters, electrodes, or mechanical elements into the propellant body.[5–9] This method requires that these elements and their electrical connectors be in physical contact with the reacting material, exposing them to damage by hot gases and sudden pressure jumps. Electromagnetic (EM) radiation provides a non-contact method to modulate material properties, potentially enabling a more convenient and robust control mechanism. Note that the idea of actively applying electromagnetic radiation during the course of an energetic reaction is distinct from simply using it for ignition. Any localized heat source, be it a flame or hot metal filament or a focused laser spot, can ignite a propellant.[10–12] Control of the reaction rate after ignition is more challenging and requires the EM radiation to be applied to the entire propellant, as opposed to a localized spot.

The most obvious mechanism for controlling the reaction rate through the application of EM radiation is to modify the temperature of the propellant. For example, EM radiation in the form of microwaves can be absorbed by metal filaments, or visible photons can be absorbed by a molecule or semiconductor in the fuel mixture. In either case, the energy contained in the EM field

is converted to heat by nonradiative relaxation, raising the local temperature. The combustion chemical reaction rates are expected to depend on temperature through the Arrhenius relation,[13] and experiments have shown a strong temperature dependence of flame propagation.[14,15] Several groups have shown that EM radiation can affect the burn rate of energetic materials,[16–18] but full spatiotemporal control of a burning sample has yet to be achieved.

In this paper, we investigate the ability of visible light to photothermally heat a high-energy Al/CuO thermite mixture and modulate its reaction rate after ignition. A thin stick of material is illuminated with a spatially varying beam, and the reaction front is imaged as it propagates along the stick. We find that the burn rate can be increased by ∼3× in the region exposed to the highest light intensity. The temperature dependence of the burn rate is analyzed in terms of the Arrhenius rate expression and effective activation energies suggest the system is limited by mass transfer. The exact mechanism of the photo-induced rate enhancement deserves further study, but the successful demonstration of control of reaction front propagation through an energetic material using laser irradiation is a promising first step in the remote control of highly exothermic reactions by light.

II. METHODS

A. Materials, precursor preparation, and direct ink writing of free-standing sticks

Aluminum nanoparticles (Al NPs, ∼100 nm, ∼92 wt. % active, determined with thermogravimetric analysis) and copper oxide nanoparticles (CuO NPs, ∼40 nm) were obtained from US Research Nanomaterials. Polyvinylidene fluoride (PVDF, average molecular weight: ∼534 000) was purchased from Sigma-Aldrich. METHOCELTM F4M hydroxypropyl methylcellulose (HPMC) was obtained from Dow Chemical Co. N,N-dimethylformamide (DMF, 99.8%) was purchased from Fisher Scientific.

The detailed procedures of direct ink writing to fabricate nanothermite composites can be found in our previous publication.[19] Therefore, only a brief description is given here. To prepare the precursor solution, a solution was made with 4 wt. % PVDF and 6 wt. % HPMC in DMF. Next a mixture of Al and CuO nanoparticles (molar Cu:Al ratio = 1.5 in order to ensure stoichiometric combustion, or an equivalence ratio of 1.0) was added to the DMF solution to make up the remaining 90 wt. %. The suspension was sonicated to form a uniform slurry. The slurry was extruded onto a glass substrate (∼75 °C) through an 18-gauge needle in a square pattern. The thickness of the resulting 1 mm wide strip ranged from 200 to 400 μm. Sticks of ∼2 cm in length were cut from the pattern and peeled off the glass substrate. A scanning electron microscope image of the cross section can be seen in Fig. S6 in the supplementary material. The porosity of the samples was ∼60% as determined by scanning electron microscopy image analysis.

B. High-speed color imaging, IR imaging, and pyrometry

In order to determine the temperature and velocity distributions across the thermite surface, two different cameras were used. First, an infrared (IR) camera was used to track the peak temperature during heating as well as the temperature distribution once the desired peak temperature was reached. Details about the operation of our IR camera (Telops, FAST M3K) can be found in previous publications.[16,20,21] Second, a high-speed color camera was used to track the position of the flame front and estimate the temperature of the flame. More information on our high-speed color imaging setup can be found in our previous publications.[22–24] Macroscopic images were taken with another high-speed color camera (Phantom Miro 110, ∼40 μm/pixel) with an aperture set at f/16, at a sample rate of 5000 fps, and an exposure time of 15 μs.

Details of the three-color[24–26] and two-color[22] imaging pyrometry can be found in our previous studies. Briefly, the raw intensities of the three-color channels (red, green, and blue) were extracted to construct color images. Ratios of the intensities of the three-color channels were used to estimate the temperature at that pixel assuming graybody emission. Calibration factors were obtained by the response to a blackbody source (ThorLabs SLS201L and Micron M390). Three-color pyrometry was not usable in these experiments because the laser irradiance at 532 nm oversaturated the green channel of the camera. As a result, only the red and blue channels were used to estimate temperature. While this did allow for temperature measurements, no uncertainty thresholding was available. Control experiments showed that the two-color measurement was consistently ∼200 K higher than the three-color method, which was within the error range of the three-color measurement. A comparison between the two and three-color pyrometry for thermites burned without the laser on can be found in Fig. S1 in the supplementary material.

C. Experimental setup

A schematic of the experimental setup is shown in Fig. 1. One end of the composite stick was clamped to an aluminum

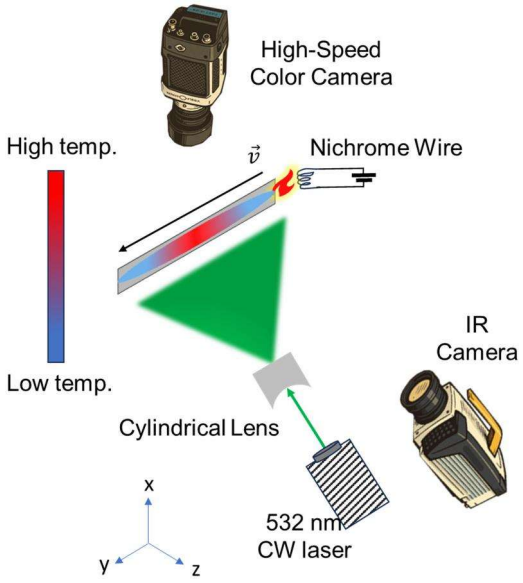

FIG. 1. Experimental setup.

frame mounted on a motorized X–Y–Z translation stage to ensure precise alignment with the laser beam. The part of the sample that was imaged for combustion testing was suspended in air to minimize heat transfer effects. Photothermal heating was performed using a continuous-wave (CW) laser operating at 532 nm with an output power of 2 W. The laser intensity was modulated using a continuously variable neutral density filter (NDL-25C-2), followed by beam expansion through a cylindrical lens (Thorlabs LK1816L1-A, focal length = −13.7 mm) to preserve the Gaussian beam profile. The unmodified laser beam (radius = 0.92 mm) was characterized using the razor blade method, and its irradiance distribution was simulated using Ansys Zemax OpticStudio to obtain the spatial irradiance profile. When heating the sticks, the peak temperature (T_{peak}) was monitored with an IR camera, and ignition was initiated once the stick held the desired peak temperature for at least one minute. To image the combustion of the thermite, the high-speed color camera was mounted perpendicular to the laser irradiation direction. Ignition of the sticks was achieved through resistive heating of a nichrome wire placed near one end of the stick.

D. Flame front tracking and local burn rate measurements

Similar measurements have already been made by our group.[16] The process used in this work differs slightly because traditional image binarization techniques proved unusable. To extract the location of the flame front, a stack of images was generated from each video and fed into Meta's Segment Anything Model 2 (SAM 2).[27] SAM 2 located the position of the flame in each image and reported the pixel location of the flame front on the thermite. Pixel position was converted to mm using the camera spatial resolution (~40 μm/pixel). Snapshots of color and segmented images can be seen in Fig. S2 in the supplementary material.

III. RESULTS AND DISCUSSION

A. Laser irradiation and surface temperature measurements

Heating of the thermite sticks was done with a 532 nm continuous-wave (CW) laser. In order to heat the surface before ignition, the beam was first passed through a neutral density filter to control the power. Second, it was expanded by a negative cylindrical lens to a diameter of 8.6 mm at the stick surface. The simulated intensity profiles are shown in Fig. 2(a) for the different laser output powers used in our experiments. Many organic high energy materials require a colored dopant, like metal nanoparticles or graphene oxide, to absorb the incoming light.[28–32] In contrast, the thermite sticks are black and opaque, with all the incident laser light either scattered or absorbed at the top surface. CuO is a small bandgap semiconductor with a penetration depth of less than 1 μm at 532 nm, so we can safely assume that light penetration into the thermite layer thickness is negligible.[33,34] For the laser powers used in these experiments, the Al/CuO sample could be stably illuminated for at least 2 min without igniting. The maximum laser power was set so that the maximum surface temperature was ~200 °C, above which the polymer binder (HPMC/PVDF) begins to degrade.[35,36]

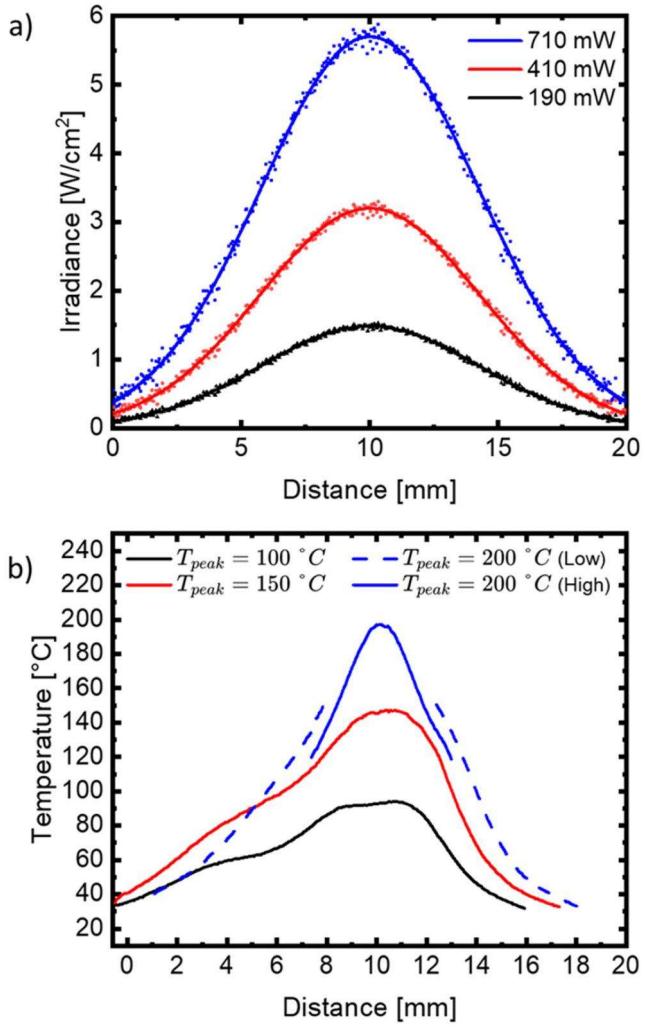

FIG. 2. (a) Simulated intensity profiles of 532 nm CW laser beam for laser powers of 133, 230, and 306 mW, corresponding to peak temperatures of ~100, 150, and 200 °C. (b) Measured temperature profiles for the three laser powers. The IR camera did not have a single temperature range setting that covered the range 25–200 °C, so two different temperature range settings were used to get the full temperature spatial profile.

Under laser irradiation, temperature profiles were monitored by an infrared (IR) camera. Typically, the thermite sticks reached a steady-state temperature distribution after <5 min of irradiation. Measured temperature profiles from the IR camera are shown in Fig. 2(b). For the highest laser power (T_{peak} = 200 °C), the IR camera could not capture the entire temperature variation without saturation, so temperature images were acquired using two different wavelength filter settings (low and high), which gave slightly different temperature readings for the same position. Another source of variation was the observation of asymmetric temperature distributions across the surface of the thermite before ignition.

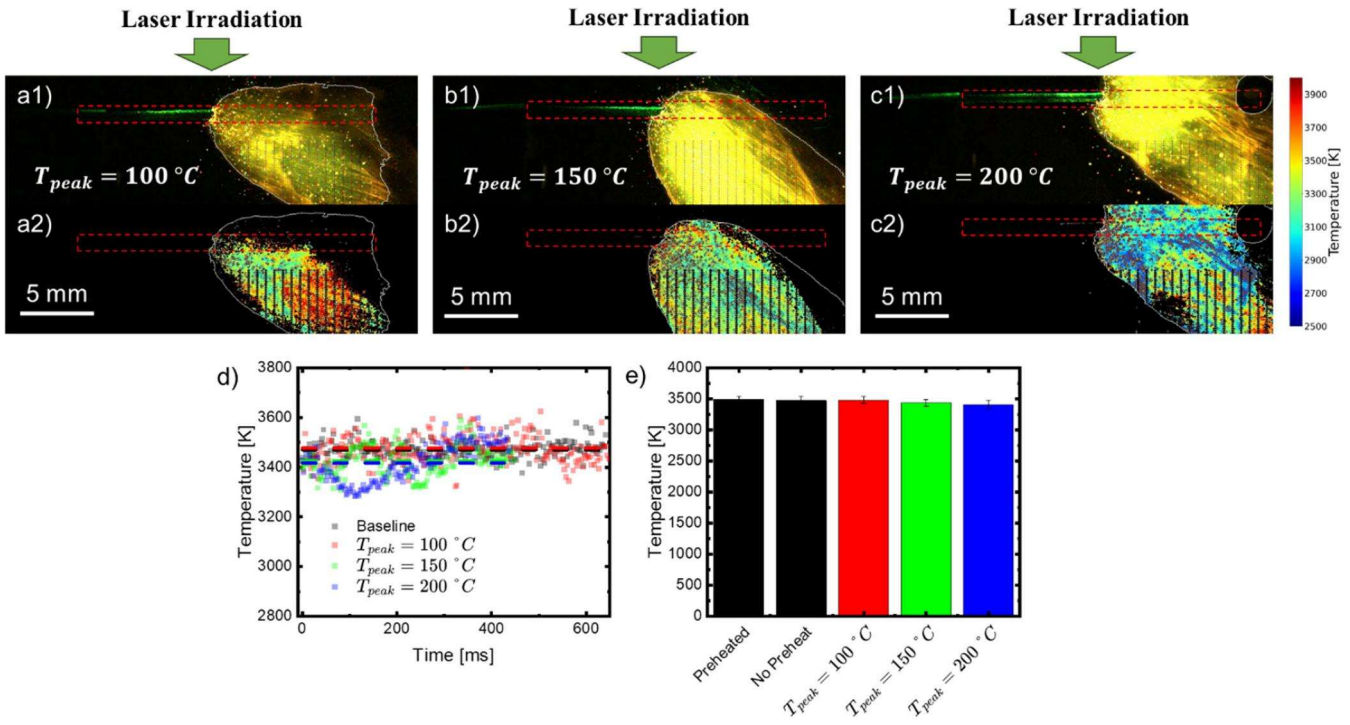

FIG. 3. Color camera (1) and corresponding two-color pyrometry (2) snapshots for peak laser temperatures of 100 (a), 150 (b), and 200 °C (c) observed along the *x*-direction in Fig. 1. The red dashed box surrounds the thermite stick, and the horizontal line of green light in the color images is scattered laser light. (d) Time dependence of the flame temperature during burn front propagation for an unirradiated sample (baseline) and the laser irradiated samples. (e) Time-averaged flame temperatures for nonirradiated samples with and without laser preheating, as well as the three different actively laser heated samples.

Similar shoulders and asymmetric profiles were observed in previous microwave heating experiments[16] and attributed to variations in surface roughness and emissivity that arise from the printing method followed by air drying. The location of the temperature shoulders varied between samples, consistent with variations in sample preparation. The peak temperature of the thermite surface increased monotonically with the laser power (Fig. S4 in the supplementary material). The full-width-half-maxima of the temperature profiles matched the laser profiles to within 10%, suggesting that photothermal heating of the stick surface gives rise to the spatially varying temperature profile of the stick. The temperature profile followed the light intensity profile closely, which we attribute to the low thermal diffusivity of the thermite composite due to grain boundaries and the organic binder. Low thermal diffusivity within the material prevents lateral (x–y coordinates) heat diffusion, allowing the laser beam profile to maintain the temperature profile at the surface. However, we expect a large temperature gradient across the 200–400 μm thickness (z coordinate). The magnitude of this gradient could not be resolved directly due to the limited spatial resolution of the thermal camera, but simulations suggest that the temperature drop across a 500 μm distance could be on the order of 100 K (Fig. S5 in the supplementary material).

B. Combustion of thermite sticks

Three-dimensional printing of the Al/CuO thermite sticks allowed us to make reproducible samples with sufficient thickness to remain free standing as the burn front propagated. Combustion tests were conducted in an open environment due to difficulties of irradiating the thermite in an anaerobic environment. Ignition was achieved by using a resistive heating element placed in contact with one end of the sample. The laser beam illuminated the top surface (referring to Fig. 1, *x* length = 20 mm, *y* length = 1 mm) of the stick, and the burn progress was monitored by a camera placed at 90° to the irradiation direction. Viewing the stick from the side (*x* length = 20 mm, *z* length = 0.2 mm) allowed us to monitor the burn propagation across the length of the stick. Combustion was initiated by resistive heating of a nichrome wire placed in contact with one end of the stick.

The use of two cameras allowed us to simultaneously monitor the position and temperature of the flame front as it propagated along the stick. Samples heated by laser irradiation to peak temperatures of 100, 150, and 200 °C were ignited. Figures 3(a1)–3(c1) show snapshots taken at the center of the stick, where the temperature peaked. When the peak temperature was 100 °C, there was no noticeable increase in the burn front velocity near the peak laser intensity. However, at the higher laser powers, there

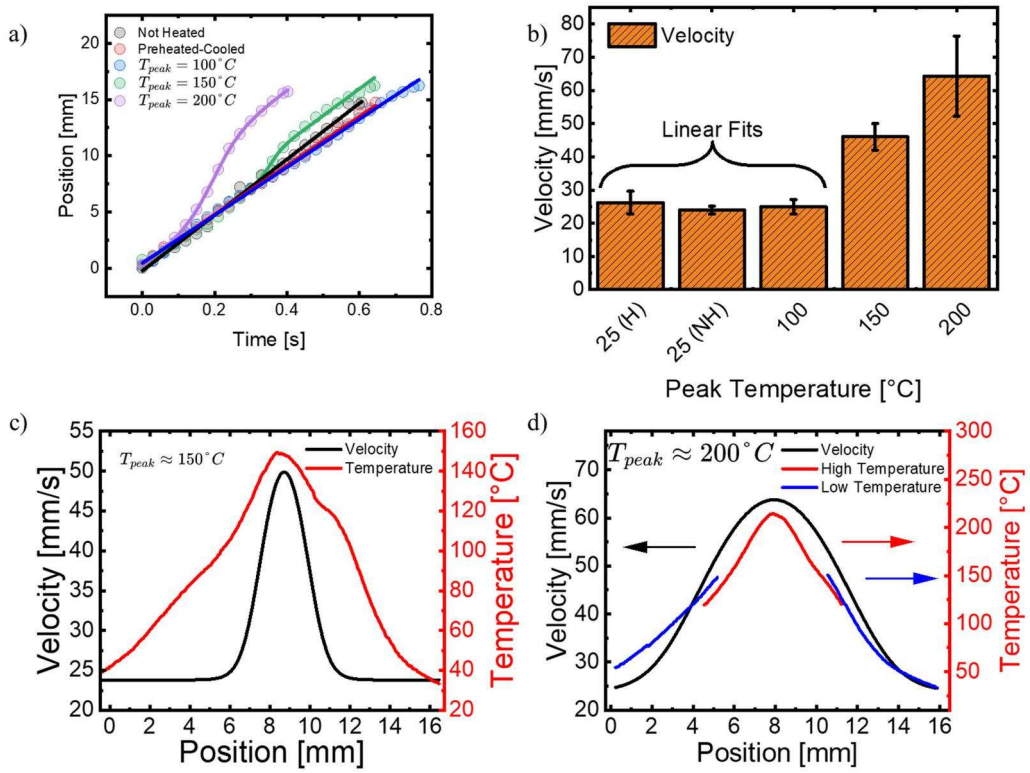

FIG. 4. (a) Time-dependent burn front position $X(t)$ for the sample conditions in Fig. 3(d). Fits using Eq. (1) are overlaid with the data. (b) Peak velocity values obtained from the fits to the $X(t)$ data. (c) Velocity $V(X)$ and temperature $T(X)$ profiles for 230 mW laser power (peak $T = 150$ °C); (d) $V(X)$ and $T(X)$ profiles for 306 mW laser power (peak $T = 200$ °C).

was a sharp increase in velocity around the point of peak laser intensity. It should be noted that the highest temperature (and the one measured by the thermal camera) is on the top of the sample, which is directly exposed to the laser light. Most of this light was absorbed in the top layer, which experienced the greatest temperature rise. The stick is suspended in air to minimize thermal loss into the surroundings, but there is still temperature gradient between top and bottom due to the different amounts of light absorbed. Consistent with this expectation, during combustion, the images showed that the burn front close to the top of the stick advanced faster than the part closer to the bottom. We did not attempt to analyze this effect, but the observation is consistent with the expected presence of a thermal gradient across the sample thickness, as mentioned above. The peak velocities through the thickness of the sample can be seen in Fig. S3 in the supplementary material.

The presence of the laser light had no effect on the final flame temperature, which was constant at ~3500 K [Figs. 3(d) and 3(e)]. It is interesting to note that Fig. 3(e) implies that any heat deposited by the laser is completely swamped by the heat evolved by the ensuing thermite reaction. To check whether laser exposure could give rise to persistent photoinduced chemical changes that might modify the combustion exothermicity, sticks were laser heated to a peak temperature of 200 °C and allowed to cool back down to room temperature. The burn rates of these sticks were compared to those that had never been heated before ignition. It was found that there was no significant difference between the two treatments, with both showing an average burn front velocity of ~24 mm/s. From these observations, we conclude that the changes in burn rate must be attributed to photothermal heating of the thermite prior to the arrival of the combustion front.

C. Local velocity and effective activation energies

In order to analyze the effects of laser exposure quantitatively, we concentrated on the top layer of the stick, whose temperature could be reliably measured. The burn front location was extracted from the high-speed video using custom software for image analysis.[27] Plots of the burn front position (X) vs time (t) are shown in Fig. 4(a). In the absence of laser heating, $X(t)$ is a linear function with an average velocity of ~24 mm/s [Fig. 4(c)]. When the laser illuminated the center of the stick to achieve a peak temperature of ~100 °C, there was no discernible acceleration as compared to linear fits to sticks without any laser heating. It was not until the peak temperature reached 150 °C that $X(t)$ became nonlinear, exhibiting a jump in the center of the stick. This deviation was

followed by a return to linearity after leaving the high temperature region. A similar pattern was achieved for 200 °C. The raw data in Fig. 4(a) have noise due to both experimental conditions (smoke and heat evolution) and the numerical procedure used to extract the burn front location. This noise could be amplified during subsequent data analysis steps, so we used an analytical function to fit $X(t)$,

$$X(t) = X_0 + V_0 t + \frac{c}{1 + e^{d(t-t_0)}}. \quad (1)$$

Equation (1) describes a tilted sigmoidal function where X_0 is the initial position, V_0 is the initial velocity in the absence of light, c is the amplitude of the jump, d is the steepness parameter that describes the steepness of the jump, and t_0 fixes the time of the maximum jump. We expect c and d to depend on the laser intensity. Qualitatively, higher light intensity leads to higher temperatures, which accelerates the burn rate and causes an earlier jump along with a larger jump in spatial position c. The parameters of the fits to Eq. (1) are given in Table I, which shows that c increases at higher laser powers while d decreases slightly. The increased c reflects a higher local velocity enhancement for 200 °C. At the highest laser intensity that yielded a peak temperature of 200 °C, the velocity increased by nearly 3× over the baseline values, as can be seen in Fig. 4(b).

Using the parameters in Table I, we can extract an analytical expression for the instantaneous velocity $V(t) = dX/dt$. Finally, we can combine the $X(t)$ and $V(t)$ data to obtain the position dependent velocity $V(X)$. Figures 4(c) and 4(d) overlay the velocity $V(X)$ and temperature $T(X)$ spatial profiles. The difference between the 150 and 200 °C data can be observed in the velocity distributions plotted in Figs. 4(c) and 4(d). The temperature distributions at 150 and 200 °C have similar widths, but the spatial velocity distribution at 200 °C is at least twice as broad, while the peak value only increases from 45 to 65 mm/s. This broadening is suggestive of a saturation of the velocity enhancement at higher intensities/temperatures.

We can combine the spatial data sets $V(X)$ and $T(X)$ to obtain the temperature dependent burn velocity $V(T)$. This approach allows us to address the mechanism of the photoinduced rate enhancement. The most obvious way to describe how a rate depends on T is the Arrhenius relation. From previous publications, it is assumed that the burn rate of a propellant is proportional to the square root of the thermal diffusivity and the reaction rate.[37,38] If we assume that the velocity is controlled by some chemical reaction (bond breaking or mass diffusion), whose rate is described by the Arrhenius equation, then the reaction front velocity is given by Eq. (2),

$$V(T) = A\exp\left[\frac{-Ea_{eff}}{2RT}\right], \quad (2)$$

where R is the ideal gas constant, A is the Arrhenius prefactor or encounter rate, and Ea_{eff} is the effective activation energy for the reaction. Based on Eq. (2), a plot of $\ln(V)$ vs $1/T$ should yield a straight line. Points where the velocity of the thermite was less than 30 mm/s were excluded from the analysis due to there being no apparent effect of preheating. As can be seen from the fits in Fig. 5, the trends for peak temperatures of 150 and 200 °C could be reasonably well described by the Arrhenius relation. But the effective activation energy decreased from ~41 to 10 kJ/mol as the

TABLE I. Relevant fitting parameters for Eq. (1) for peak temperatures of 150 and 200 °C.

Peak temperature (°C)	V_0 (mm/s)	c (mm)	d (1/s)
150	23.8	2.8 ± 1.8	42.0 ± 17.6
200		5.1 ± 0.8	32.5 ± 11.1

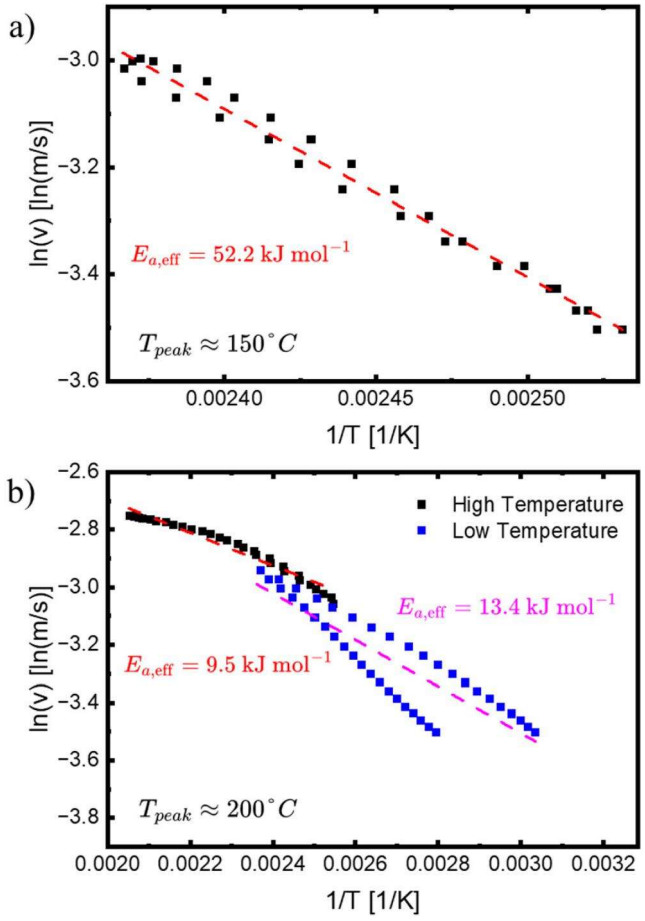

FIG. 5. (a) Example Arrhenius plot of $V(T)$ data from a single run for laser power 230 mW (peak $T = 150$ °C). (b) Example Arrhenius plot of $V(T)$ data from a single run for laser power 306 mW (peak $T = 200$ °C). Because the IR temperature measurements were performed across two ranges [see Fig. 2(b)], the Ea_{eff} analysis was done separately for each range. The red line and text correspond to the high temperature range, and the pink line and text correspond to the low temperature range.

TABLE II. Average and standard deviations of activation energies estimated over three runs, including those shown in Fig. 5. The value in parentheses for 200 °C corresponds to the low temperature range from the IR camera.

Peak temperature (°C)	Activation energy (kJ/mol)
150	40.5 ± 19.3
200	9.8 ± 4.4
200 (Low temp)	(19.7 ± 10.3)

peak temperature increased from 150 to 200 °C. Average Ea_{eff} values with standard deviations are given in Table II.

From the Arrhenius analysis, we can make three main observations. First, the fact that the data analysis yielded reasonably linear Arrhenius plots suggests that this physical model can be applied to such systems. There are many options for analyzing temperature dependent rate processes,[39,40] but to be consistent with our previous work, we elected to use the simplest Arrhenius model [Eq. (2)]. More sophisticated models might yield better agreement with the data, but at the cost of more complicated physical interpretation. Second, the Ea_{eff} values are roughly an order of magnitude lower than the reported value for the CuO thermite combustion activation energy of ~270 kJ/mol.[41] The lower Ea_{eff} values may reflect the presence of the PVDF in the composite, which has been shown to accelerate Al combustion.[42–44] Alternatively, we have previously attributed a relatively low Ea_{eff} in similar systems to an activated mass transfer process that acts as the rate-limiting step.[16] The third observation is that the Ea_{eff} value at 200 °C is 4× lower than the value obtained at 150 °C. This observation suggests a change in material properties between the two temperatures. Both polymer binders undergo phase transitions in this range, with PVDF melting[45] and HPMC undergoing a glass transition.[46] If the mass transport is accelerated at 200 °C due to increased polymer fluidity, this would facilitate contact between the CuO and Al particles and enhance combustion. The lower Ea_{eff} would reflect this improved transport at 200 °C. On the other hand, if Ea_{eff} is even higher at $T_{peak} = 100$ °C, this might explain the lack of laser-induced acceleration we see at that value of T_{peak}. A higher Ea_{eff} would mean that the smaller temperature increase would be unable to induce a significant change in rate. For example, from Fig. 4(c) a temperature of 100 °C cannot induce a change in velocity, while in Fig. 4(d) it can. From a fundamental perspective, this apparent variation of Ea_{eff} with temperature indicates the inadequacy of the Arrhenius equation (since activation energies are usually assumed to be independent of temperature) and points to the need for more sophisticated models. The physical origin of the temperature dependence of V will have to be clarified by future experiments. It is notable, however, that laser heating provides a new way to probe the temperature-dependent reactivity of this complex mixture. The ability to vary sample temperature *in situ* may reveal new phenomena in the solid-state combustion process.

Last, we consider some practical implications of this work. Our results show how 532 nm laser preheating provides a way to imprint a burn rate pattern onto a thermite fuel. This pattern exists in all three dimensions: the temperature variation along length (x axis) and width (y axis) will mirror the laser beam profile, while the thickness (z axis) variation depends on the laser penetration depth. In principle, shaping the beam xy profile and tuning the laser wavelength should enable us to imprint different three-dimensional temperature profiles into the material. For example, longer wavelength light will have a deeper penetration depth and generate a smaller gradient along the thickness (z axis). Increasing the laser intensity will decrease the time required to reach a chosen temperature, but care must be taken not to prematurely ignite the illuminated region of material. To achieve active control of the burn front as it propagates through a macroscopic fuel sample, like a rocket engine, would likely require real-time feedback to adjust the laser intensity profile to maintain the desired temperature in the unburned material. One way to implement such control would be to switch from side illumination (perpendicular to the burn front propagation direction) to illumination parallel to the propagation direction. In this geometry, the laser would follow the burn front and modulate its cross-sectional shape and propagation rate. This approach would require a higher laser intensity to rapidly heat the surface that is continuously exposed as the combustion front moves through the material. It would also require light delivery along the axis of propagation, a problem that has been addressed in a recent paper.[47] Clearly, the proof-of-principle experiments in this paper will require additional development before laser controlled combustion can become a practical tool.

IV. CONCLUSION

In this paper, we used a standard laser source at 532 nm to control burn front propagation across a thermite propellant similar to that used in rocket fuels. Real-time imaging of the burn front showed a 3× enhancement in the burn rate at the highest laser powers that generated a peak surface temperature of ~200 °C. Parallel measurements of the spatial dependence of the flame front velocity and temperature enabled us to estimate effective activation energies of thermite burn front propagation. This analysis suggests that laser preheating enhances the mass transport properties of the composite, as opposed to the chemical combustion reaction. Although there are still some unanswered questions, this proof-of-principle experiment is a promising step in developing non-contact methods to control the thermite combustion and eventually the thrust of a solid propellant rocket.

SUPPLEMENTARY MATERIAL

See the supplementary material for a comparison of the three and two-color pyrometry, color and segmented images for reaction zone tracking, burn speeds through the thickness of the thermite samples, and peak surface temperatures and corresponding laser powers.

ACKNOWLEDGMENTS

This work was supported by the National Science Foundation, Grant No. DMR-1810514.

AUTHOR DECLARATIONS

Conflict of Interest

The authors have no conflicts to disclose.

Author Contributions

Touhid Bin Anwar and Erik Hagen contributed equally to this study.

Touhid Bin Anwar: Data curation (equal); Formal analysis (equal); Writing – original draft (equal). **Erik Hagen:** Data curation (equal); Formal analysis (equal); Writing – original draft (equal). **Keren Shi:** Data curation (equal). **Michael R. Zachariah:** Conceptualization (equal); Funding acquisition (equal); Investigation (equal); Methodology (equal); Project administration (equal); Resources (equal); Supervision (equal); Writing – review & editing (equal). **Christopher J. Bardeen:** Conceptualization (equal); Funding acquisition (equal); Investigation (equal); Methodology (equal); Project administration (equal); Resources (equal); Supervision (equal); Writing – review & editing (equal).

DATA AVAILABILITY

The data that support the findings of this study are available within the article and its supplementary material available online.

REFERENCES

[1]K. E. Uhlenhake, M. Gomez, D. N. Collard, M. Örnek, and S. F. Son, "Laser ignition of solid propellants using energetic nAl-PVDF optical sensitizers," Combust. Flame **254**, 112848 (2023).

[2]D. M. Badgujar, M. B. Talawar, S. N. Asthana, and P. P. Mahulikar, "Advances in science and technology of modern energetic materials: An overview," J. Hazard. Mater. **151**, 289–305 (2008).

[3]W. Li, W. Li, Y. He, and G. Liang, "Reverse design of solid propellant grain for a performance-matching goal: Shape optimization via evolutionary neural network," Aerospace **9**, 552 (2022).

[4]E. Kim, S. Joo, and S. Oh, "Inverse design framework for optimizing solid propellant grains toward target performance profiles," Acta Astronaut. **238**, 645–656 (2026).

[5]Z. Wang, F. Li, Q. Zhang, L. Li, K. Ouyang, R. Shen, Y. Ye, L. T. DeLuca, and W. Zhang, "Electrically controlled solid chemical propulsion: A review," Chem. Eng. J. **496**, 154100 (2024).

[6]D. K. Messer, C. T. Nunes, M. Örnek, and S. F. Son, "Throttleable solid propellants through embedded shape memory alloy and resistance wires," Propell. Explos. Pyrotech. **50**(3), e202400251 (2025).

[7]C. T. V. Nunes, M. Örnek, T. A. Hafner, and S. F. Son, "Enhanced piezoelectric performance of Al/P(VDF-TrFE) nanocomposite films for energetic sensors and ignitors," J. Appl. Phys. **138**(11), 114901 (2025).

[8]B. Gobin, P. Reiter, S. Whalen, and G. Young, "Extinguishing and combustion characteristics of electrically controllable solid propellants under elevated pressures," J. Propul. Power **40**(1), 152–163 (2024).

[9]Y. Li, H.-Y. Lv, S.-W. Song, Q.-L. Yan, and Q.-H. Zhang, "Recent advances on electrically controlled solid propellants," Fuel **394**, 135096 (2025).

[10]N. K. Bourne, "On the laser ignition and initiation of explosives," Proc. R. Soc. London Ser., A **457**(2010), 1401–1426 (2001).

[11]Z. Alibay, D. J. Kline, M. C. Rehwoldt, P. Biswas, S. Herrera, H. Wang, and M. R. Zachariah, "Mechanism of microwave-initiated ignition of sensitized energetic nanocomposites," Chem. Eng. J. **415**, 128657 (2021).

[12]X. Fang and J. Akhavan, "Review on laser initiation of energetic materials," Propell. Explos. Pyrotech. **50**(5), e12037 (2025).

[13]D. M. Golden and J. R. Barker, "Pressure- and temperature-dependent combustion reactions," Combust. Flame **158**(4), 602–617 (2011).

[14]A. I. Atwood, T. L. Boggs, P. O. Curran, T. P. Parr, D. M. Hanson-Parr, C. F. Price, and J. Wiknich, "Burning rate of solid propellant ingredients, part 2: Determination of burning rate temperature sensitivity," J. Propul. Power **15**(6), 748–752 (1999).

[15]J. A. Condon, J. P. Renie, and J. R. Osborn, "Temperature sensitivity of propellant burning rates," Combust. Flame **30**, 267–276 (1977).

[16]K. Shi, Y. Wang, and M. R. Zachariah, "Microwave antenna focusing for spatially resolved modulation of burn rate," Chem. Eng. J. **492**, 152192 (2024).

[17]X. Zang, J. Cheng, J. Xu, M. Gozin, Y. Ye, and R. Shen, "Interactions between microwaves and smart energetic materials: A review on emerging technologies for ignition and combustion enhancement," Chem. Eng. J. **498**, 155031 (2024).

[18]B. Duan, H. Zhang, L. Wu, Z. Hua, Z. Bao, N. Guo, Y. Ye, and R. Shen, "Controllable combustion behaviors of the laser-controlled solid propellant," Def. Technol. **18**(1), 38–48 (2022).

[19]H. Wang, J. Shen, D. J. Kline, N. Eckman, N. R. Agrawal, T. Wu, P. Wang, and M. R. Zachariah, "Direct writing of a 90 wt. % particle loading nanothermite," Adv. Mater. **31**(23), 1806575 (2019).

[20]Y. Wang, M. Chowdhury, Y. Zhou, G. Issac Paul, K. Shi, and M. R. Zachariah, "Oscillating-to-continuous combustion transition in mesoparticle composites through manipulation of heat feedback," Adv. Funct. Mater. **34**(42), 2406722 (2024).

[21]K. Shi, M. Bokhoor, Y. Wang, T. P. Weihs, and M. R. Zachariah, "Propagation rate and product modulation in SHS reactions via focused microwave heating," Chem. Eng. Sci. **302**, 120794 (2025).

[22]Y. Wang, E. Hagen, P. Biswas, H. Wang, and M. R. Zachariah, "Imaging the combustion characteristics of Al, B, and Ti composites," Combust. Flame **252**, 112747 (2023).

[23]H. Wang, B. Julien, D. J. Kline, Z. Alibay, M. C. Rehwoldt, C. Rossi, and M. R. Zachariah, "Probing the reaction zone of nanolaminates at ∼μs time and ∼μm spatial resolution," J. Phys. Chem. C **124**(25), 13679–13687 (2020).

[24]R. J. Jacob, D. J. Kline, and M. R. Zachariah, "High speed 2-dimensional temperature measurements of nanothermite composites: Probing thermal vs. Gas generation effects," J. Appl. Phys. **123**(11), 115902 (2018).

[25]D. J. Kline, M. C. Rehwoldt, J. B. DeLisio, S. C. Barron, H. Wang, Z. Alibay, J. C. Rodriguez, G. M. Fritz, and M. R. Zachariah, "In-operando thermophysical properties and kinetics measurements of Al-Zr-C composites," Combust. Flame **228**, 250–258 (2021).

[26]Q. Meng, E. Hagen, C. Goodman, M. A. Foster, and M. R. Zachariah, "Simultaneous hyperspectral imaging and pyrometry for multi-phase temperature profiling of energetic composite reactions," J. Quant. Spectrosc. Radiat. Transf. **346**, 109598 (2025).

[27]N. Ravi, V. Gabeur, Y.-T. Hu, R. Hu, C. Ryali, T. Ma, H. Khedr, R. Rädle, C. Rolland, L. Gustafson, E. Mintun, J. Pan, V. Alwala, N. Carion, C.-Y. Wu, R. Girshick, P. Dollár, and C. Feichtenhofer, "SAM 2: Segment anything in images and videos," arXiv:2408.00714 (2024).

[28]X. Fang, M. Sharma, C. Stennett, and P. P. Gill, "Optical sensitisation of energetic crystals with gold nanoparticles for laser ignition," Combust. Flame **183**, 15–21 (2017).

[29]X. Fang, M. Stone, and C. Stennett, "Pulsed laser irradiation of a nanoparticles sensitised RDX crystal," Combust. Flame **214**, 387–393 (2020).

[30]X. R. Shi, L. F. Yang, L. Tian, J. P. Shen, Z. Q. Li, and C. H. Pei, "Laser ignited combustion of mesoporous nitrocellulose/graphene oxide composite aerogel with strong photo-thermal sensitivity and high flame propagation rate," J. Appl. Phys. **130**(22), 225105 (2021).

[31]J. H. Kim, J. Y. Ahn, H. S. Park, and S. H. Kim, "Optical ignition of nanoenergetic materials: The role of single-walled carbon nanotubes as potential optical igniters," Combust. Flame **160**(4), 830–834 (2013).

[32]J. Yan, X. Zhang, X. Li, R. Baghi, B. L. Weeks, and L. J. Hope-Weeks, "Facile incorporation of optical sensitizers into nitrocellulose aerogels for improved laser ignition and combustion," Adv. Compos. Hybrid Mater. **7**(6), 242 (2024).

[33]J. Mahl, S. Neppl, F. Roth, M. Borgwardt, C. Saladrigas, B. Toulson, J. Cooper, T. Rahman, H. Bluhm, J. Guo, W. Yang, N. Huse, W. Eberhardt, and O. Gessner, "Decomposing electronic and lattice contributions in optical pump—X-ray probe transient inner-shell absorption spectroscopy of CuO," Faraday Discuss. **216**(0), 414–433 (2019).
[34]H. Wieder and A. W. Czanderna, "Optical properties of copper oxide films," J. Appl. Phys. **37**(1), 184–187 (1966).
[35]H. N. Giang, A. T. K. Le, T. N. A. Huynh, T. K. Phung, and W. Sakai, "Effect of additives on fabrication and properties of hydroxypropyl methylcellulose-based hydrogels," Polym. Bull. **80**(10), 11121–11137 (2023).
[36]M. C. Rehwoldt, Y. Wang, F. Xu, P. Ghildiyal, and M. R. Zachariah, "High-temperature interactions of metal oxides and a PVDF binder," ACS Appl. Mater. Interfaces **14**(7), 8938–8946 (2022).
[37]C. K. Law, *Combustion Physics* (Cambridge University Press, 2010).
[38]Mallard and L. Chatelier, "Recherches sur la combustion des mélanges gazeux explosifs," J. Phys. Theor. Appl. **4**(1), 59–84 (1885).
[39]M. J. Starink, "The determination of activation energy from linear heating rate experiments: A comparison of the accuracy of isoconversion methods," Thermochim. Acta **404**(1–2), 163–176 (2003).
[40]S. Hu, X. Liu, L. Liu, B. Kang, and Y. Zhang, "Effects of metal oxides on the thermal decomposition kinetics and mechanisms of HAN/PVA based propellants," Cent. Europ. J. Energetic Mater. **18**, 322–328 (2021).
[41]S. M. Umbrajkar, M. Schoenitz, and E. L. Dreizin, "Exothermic reactions in Al–CuO nanocomposites," Thermochim. Acta **451**(1–2), 34–43 (2006).
[42]J. Jiang, X.-H. Ju, and Z. Mei, "Mechanistic insights into combustion enhancement of PVDF-encapsulated pure aluminum nanoparticles: A ReaxFF molecular dynamics study," Appl. Surf. Sci. **719**, 165128 (2026).
[43]Y. Xun, L. Yan, Y. Sun, X. Li, H. Feng, and K. Ma, "Mechanism study on enhancing the combustion performance of aluminum with polyvinylidene fluoride," Phys. Chem. Chem. Phys. **27**(42), 22575–22587 (2025).
[44]K. E. Uhlenhake, D. N. Collard, A. C. Hoganson, A. D. Brown, S. Fox, M. Örnek, J. F. Rhoads, and S. F. Son, "Additively manufactured micro- and nano- Al/PVDF ignition sensitivity and burning characterization," Propell. Explos. Pyrotech. **48**(4), e202200204 (2023).
[45]J. E. Marshall, A. Zhenova, S. Roberts, T. Petchey, P. Zhu, C. E. J. Dancer, C. R. McElroy, E. Kendrick, and V. Goodship, "On the solubility and stability of polyvinylidene fluoride," Polymers **13**(9), 1354 (2021).
[46]H. McPhillips, D. Q. M. Craig, P. G. Royall, and V. L. Hill, "Characterisation of the glass transition of HPMC using modulated temperature differential scanning calorimetry," Int. J. Pharmaceut. **180**(1), 83–90 (1999).
[47]Y. Zhou, L. Yang, K. Shi, and M. R. Zachariah, "Optically transparent solid-fuel to couple energy to the regression front," Fuel **405**, 136476 (2026).